

## ARTICLE OPEN



## ACUTE LYMPHOBLASTIC LEUKEMIA

The EGR3 regulome of infant *KMT2A*-r acute lymphoblastic leukemia identifies differential expression of B-lineage genes predictive for outcome

Marius Külp<sup>1,2</sup>, Patrizia Larghero<sup>1</sup>, Julia Alten<sup>3</sup>, Gunnar Cario<sup>3</sup>, Cornelia Eckert<sup>4</sup>, Aurélie Caye-Eude<sup>5,6</sup>, Hélène Cavé<sup>5,6</sup>, Tessa Schmachtel<sup>2</sup>, Michela Bardini<sup>7</sup>, Giovanni Cazzaniga<sup>7,8</sup>, Paola De Lorenzo<sup>9</sup>, Maria Grazia Valsecchi<sup>10</sup>, Halvard Bonig<sup>11,12,13</sup>, Claus Meyer<sup>1</sup>, Michael A. Rieger<sup>2,14,15</sup> and Rolf Marschalek<sup>1</sup>

© The Author(s) 2023

*KMT2A*-rearranged acute lymphoblastic infant leukemia (*KMT2A*-r iALL) is associated with outside risk of relapse and relapse mortality. We previously reported strong upregulation of the immediate early gene *EGR3* in *KMT2A::AFF1* iALL at relapse; now we provide analyses of the *EGR3* regulome, which we assessed through binding and expression target analysis of an *EGR3*-overexpressing t(4;11) cell culture model. Our data identify *EGR3* as a regulator of early B-lineage commitment. Principal component analysis of 50 *KMT2A*-r iALL patients at diagnosis and 18 at relapse provided strictly dichotomous separation of patients based on the expression of four B-lineage genes. Absence of B-lineage gene expression translates to more than two-fold poorer long-term event-free survival. In conclusion, our study presents four B-lineage genes with prognostic significance, suitable for gene expression-based risk stratification of *KMT2A*-r iALL patients.

*Leukemia* (2023) 37:1216–1233; <https://doi.org/10.1038/s41375-023-01895-z>

## INTRODUCTION

Seventy to eighty percent of iALL are *KMT2A*-rearranged (*KMT2A*-r); an association with inferior survival was noted and independently confirmed [1, 2]. 49% of *KMT2A*-r iALL possess the translocation t(4;11)(q21;q23) generating the fusion oncogenes *KMT2A::AFF1* and *AFF1::KMT2A* [3]. On-treatment relapse is frequent and mortality is high [1, 2, 4]. Despite the successful implementation of targeted therapies in pediatric leukemia, a relapse-preventing iALL therapy remains to be established.

Our group recently reported the immediate early gene *Early Growth Response 3* (*EGR3*) as relapse-associated, with 100-fold increased *EGR3* gene expression levels at the time of relapse compared to primary diagnosis [5]. This prompted us to investigate the role of *EGR3* in the context of *KMT2A::AFF1* iALL in more detail.

*EGR3* belongs to the family of C2H2 zinc finger transcription factors with high structural and functional relation to *EGR1* and

*EGR2* [6, 7]. *EGR* proteins act as direct transcriptional activators and repressors, with the ability to recruit NAB proteins as coregulators [8–11]. Functionally, the *EGR* genes were related to neuronal development [12–16], hematopoietic stem cell quiescence [17, 18], and development of T and B cells [19–21].

Here we explore the *EGR3* regulome of *KMT2A::AFF1* proB-ALL in detail through integration of data derived from massive analysis of cDNA ends-sequencing (MACE-Seq) and chromatin immunoprecipitation DNA-sequencing (ChIP-Seq) of an *EGR3*-overexpression SEM cell model. Our study identifies *EGR3* as a regulator of early B-lineage specification and commitment. Additionally, gene expression and principal component analysis of 50 *KMT2A*-r iALL patients at diagnosis and 18 at relapse provides strictly bimodal clustering of patients based on the expression of the identified B-lineage genes. Absence of B-lineage gene expression translates to dismal outcome with more than two-fold poorer long-term event-free survival.

<sup>1</sup>Diagnostic Center of Acute Leukemia (DCAL), Institute of Pharmaceutical Biology, Goethe-University, Frankfurt am Main, Germany. <sup>2</sup>Department of Medicine, Hematology/Oncology, Goethe University Hospital Frankfurt, Frankfurt am Main, Germany. <sup>3</sup>Department of Pediatrics, University Medical Center Schleswig-Holstein, Campus Kiel, Germany. <sup>4</sup>Department of Pediatric Hematology and Oncology, Charité-Universitätsmedizin Berlin, Berlin, Germany. <sup>5</sup>Genetics Department, AP-HP, Hôpital Robert Debré, F-75019 Paris, France. <sup>6</sup>Université Paris Cité, Inserm U1131, Institut de recherche Saint-Louis, F-75010 Paris, France. <sup>7</sup>Centro Ricerca Tettamanti, Pediatrics, University of Milan-Bicocca, Fondazione Monza e Brianza per il Bambino e la sua Mamma (MBBM)/San Gerardo Hospital, Monza, Italy. <sup>8</sup>Genetics, School of Medicine and Surgery, University of Milan-Bicocca, Monza, Italy. <sup>9</sup>Statistical Section, Pediatric Clinic, University of Milan-Bicocca, Monza, Italy. <sup>10</sup>Center of Bioinformatics, Biostatistics and Bioimaging, University of Milan-Bicocca, Monza, Italy. <sup>11</sup>Institute for Transfusion Medicine and Immunohematology, Goethe University, Frankfurt am Main, Germany. <sup>12</sup>German Red Cross Blood Service Baden-Württemberg-Hessen, Frankfurt am Main, Germany. <sup>13</sup>Department of Medicine, Division of Hematology, University of Washington School of Medicine, Seattle, WA, USA. <sup>14</sup>German Cancer Consortium (DKTK) and German Cancer Research Center (DKZF), Heidelberg, Germany. <sup>15</sup>Cardio-Pulmonary Institute, Frankfurt am Main, Germany.

<sup>✉</sup>email: marius.kuelp@em.uni-frankfurt.de; rolf.marschalek@em.uni-frankfurt.de

Received: 21 December 2022 Revised: 28 March 2023 Accepted: 31 March 2023

Published online: 26 April 2023

## METHODS

### Cell culture

Establishment of the cell lines SEM::EGR3 and SEM::mock with Doxycycline-inducible transgene expression is described in our former study [5]. SEM cells were cultivated under sterile conditions and maintained in RPMI 1640 (RPMI-HA, Capricorn Scientific) supplemented with 10% FBS (FBS-11A, Capricorn Scientific), 2 mM L-glutamine (STA-B, Capricorn Scientific), 100 U/ml penicillin and 100 µg/ml streptomycin (PS-B, Capricorn Scientific), preheated to 37 °C prior to use. Cells were kept at 37 °C in 5% CO<sub>2</sub> and a relative humidity of 95%. SEM cells were passaged twice a week keeping a density of ~1–3 × 10<sup>6</sup> cells/mL. Cell lines are tested on a regular basis.

### Gene expression analysis using qRT-PCR of patient samples

Informed consent was obtained for all patients through the respective study center, which provided patient RNA. Analyzed patients displayed a proB phenotype and were diagnosed between 0 and 12 months of age (infants). RNA was extracted from peripheral blood at the day of diagnosis (dx cohort, *n* = 50) or relapse (rel cohort, *n* = 18) by the respective study center. cDNA was synthesized out of 1 µg RNA using random hexamer N6 primers and SuperScript™ II Reverse Transcriptase (18064071, invitrogen). The dx cohort is composed of *KMT2A::AFF1* iALL cases (Table 1), the rel cohort is composed of different *KMT2A-r* iALLs (Table 2). *IGHM*, *CD79A*, *BLK*, and *PTPN6* gene expression was measured as technical triplicates using qRT-PCR (StepOnePlus system) and ΔC<sub>T</sub> mean values were calculated using *GAPDH* expression as a reference. Relative expressions were calculated as ratio (reference/target) = 2<sup>CT(GAPDH) - CT(target)</sup> = 2<sup>-ΔCT</sup>. If available, clinical outcome was provided by the study centers. Used oligonucleotides are described in Table 3. The *EGR3* expression data were already assessed during our former study with the same cohorts [5]. Pearson correlations were calculated using GraphPad Prism software.

### Flow cytometry of SEM::EGR3 and SEM::mock

Cells were blocked using Human BD Fc Block™ (BD) and stained with FACS antibodies (BD) according to the manufacturer's protocol. Cells were analyzed using a BD FACSVerse™. Cells of interest were gated out of all cells using FSC-H and FSC-A. Subsequently, single cells were gated and assessed for CD19, IgM and CD79A protein surface expressions with gates set using fluorescence minus one (FMO) controls. Flow cytometric analysis was performed with four biological replicates of SEM::mock and SEM::EGR3 on a BD FACSaria™ III Cell Sorter. FACS plots were created using FlowJo™ Software. Antibodies used for flow cytometry are described in Table 4.

### Massive analysis of cDNA ends-sequencing (MACE-Seq)

MACE-Seq is 3' single end mRNA sequencing enabling high resolution transcription profiling of RNA extracted from three biological replicates of SEM::mock and SEM::EGR3 48 h after induction with Doxycycline 1 µg/mL. Screen tape analysis of RNA was performed using the bioanalyzer Agilent 2200 TapeStation assessing the RNA integrity number (RIN). RIN values above 8.5 were considered as tolerable. MACE-Seq of extracted RNAs was performed by GenXPro GmbH. MACE-Seq data are available at GEO with accession code GSE225710.

### Chromatin immunoprecipitation DNA-sequencing (ChIP-Seq)

ChIP-Seq data of SEM::EGR3 immunoprecipitated with an α-FLAG antibody in comparison to input were already obtained during our former study (GSE205652). ChIP-Seq data are available at GEO with accession code GSE205652.

### Statistics and data analysis

Appropriate statistical tests were performed within *DeSeq2*, *GSEA*, or *BETA plus* algorithms in context of differential expression and gene set enrichment analyses of MACE-Seq data or binding and expression target analysis of ChIP- and MACE-Seq data, respectively. The level of significance is indicated by *p* values (*DeSeq2*), false discovery rates (*GSEA*) or rank products (*BETA plus*). Used expression and binding data meet the demands of respective algorithms and associated statistical tests in terms of normality and equal-variance assumptions. The phenotypic populations assessed by flow cytometry were compared using two-tailed *t* tests performed using GraphPad Prism 9.5.0 software. Principal component

analyses (PCA) were conducted as singular value decompositions using ClustVis [22] with applied unit variance scaling for rows.

Sample sizes were chosen depending on experimental context. qRT-PCR was performed as technical triplicates of 68 patient samples in total. MACE-Seq was performed using three biological triplicates of SEM::mock and SEM::EGR3 RNA. Flow cytometric analysis was performed using four biological replicates of SEM::mock and SEM::EGR3.

Gene set enrichment analysis (GSEA) was conducted using GSEA 4.2.3 according to the developer's protocol [23].

Integration of MACE-Seq and ChIP-Seq data as well as transcription factor motif scanning was performed using the online tool BETA plus according to the developer's protocol [24].

The 3890 up- and 3107 downregulated direct *EGR3* target genes identified with BETA were uploaded to the PANTHER 17.0 classification system [25]. The functional classification considering protein class, biological function/gene ontology (GO) term, and chromosomal location was plotted using Microsoft Excel as net plots.

Survival analysis was performed using GraphPad Prism 9.4.1. Event-free survival (EFS) was defined as the time from diagnosis to first failure including induction failure, relapse, death, or second malignant neoplasm according to the Interfant-99 protocol [2]. Time was censored at last follow-up if no events were observed. Curves were computed with the Kaplan–Meier estimator, standard errors (SE) with the Greenwood formula, and curves were compared with the log-rank test.

## RESULTS

### Overexpression of *EGR3* in the *KMT2A::AFF1* proB cell line SEM upregulates B-lineage specification and commitment genes

We recently identified *EGR3* as a relapse-associated factor in *KMT2A-r* iALL, whose gene expression is ~100-fold increased in patients at relapse (rel) compared to primary diagnosis (dx) [5]. Surprisingly, re-analysis of the Leukemia MILE study data involving 2096 patient samples using the online database BloodSpot revealed B cell malignancies to be characterized by a decreased *EGR3* gene expression in comparison to healthy bone marrow (BM) (Supplementary Fig. 1A) [26, 27]. Regarding healthy hematopoietic cells, the BloodSpot DMAP dataset demonstrates low *EGR3* expression in proB cells which strongly elevates with differentiation to naïve B cells and their progeny (Supplementary Fig. 1B) [28].

Accordingly, the inducible *EGR3* overexpression SEM cell model (SEM::EGR3) of our previous study represents the cellular identity of leukemic blasts in relapsed patients, with a proB phenotype, a strongly increased *EGR3* gene expression, and the *KMT2A::AFF1* genotype. To ascertain the role of *EGR3* in disease progression and relapse, we performed massive analysis of cDNA ends-sequencing (MACE-Seq) of SEM::EGR3 and the corresponding empty vector control cell line SEM::mock. MACE-Seq and differential gene expression analysis using *DeSeq2* identified 10,645 differentially expressed genes between SEM::EGR3 and SEM::mock, referred to as the *EGR3* transcriptome. 6082 genes were up- and 4563 downregulated (log<sub>2</sub> > or < 0, *p* < 0.05). A set of B-lineage genes was found to be strongly overexpressed (*IGHM* (log<sub>2</sub>fc = 11.42), *CD79A* (log<sub>2</sub>fc = 6.84), *BLK* (log<sub>2</sub>fc = 8.55), *PTPN6* (log<sub>2</sub>fc = 7.16), *CD22* (log<sub>2</sub>fc = 6.42), *CD19* (log<sub>2</sub>fc = 5.21), *IGLL1* (log<sub>2</sub>fc = 8.91)).

Gene set enrichment analysis (GSEA) was used to functionally characterize the *EGR3* transcriptome considering 13,938 gene sets, of which 9910 were significantly enriched in the phenotype *EGR3* at a nominal *p* value below 0.01. 'Signaling by the B cell receptor' (Reactome, R-HSA-983705) was identified as the highest ranked gene set (NES = 2.96, FDR = 0.050) (Table 5, Fig. 1A, D). This was corroborated by the B cell receptor (BCR) signaling gene sets of Wiki Pathways (NES = 2.73, FDR = 0.050) (Fig. 1B, E) and the Pathway Interaction Database (NES = 2.61, FDR = 0.050) (Fig. 1C, F) being at ranks four and 18, respectively [29–31]. The top scored upregulated genes in the three sets were *IGHM*, *CD79A*, *BLK*, *PTPN6*, *CD22*, and *CD19* (Fig. 1D–F). Importantly, also the pre-BCR surrogate light chain gene *IGLL1* was found to be

**Table 1.** Patient characteristics of the dx cohort (*n* = 50).

Patient no.	Patient age [months]	Treatment protocol	sex	Time to event (last follow-up) [months]	% blasts	EGR3 ΔC <sub>T</sub> Mean	IGHM ΔC <sub>T</sub> Mean	CD79A ΔC <sub>T</sub> Mean	BLK ΔC <sub>T</sub> Mean	PTPN6 ΔC <sub>T</sub> Mean	HOXA9ΔC <sub>T</sub> Mean
1	5.0	Interfant-06	F	(40.1)	49	8.1850	3.9578	2.6439	5.1517	3.8854	13.3592
2	6.0	/	F	/	82	11.2758	4.1454	2.2853	4.3700	2.1229	3.9204
3	2.0	Interfant-06	F	(23.6)	46	9.3618	4.8963	2.7340	4.4007	4.4306	12.9546
4	6.0	Interfant-06	M	(17.1)	90	11.1637	9.1284	7.8716	9.8465	10.1343	11.5783
5	10.0	/	M	/	90	8.8214	5.4178	6.2042	10.2556	9.6764	3.5974
6	2.0	Interfant-06	M	(83.6)	95	11.5618	6.2522	6.9626	8.1896	8.8812	4.9698
7	3.0	Interfant-06	F	(5.6)	96	8.5196	5.8631	2.8374	-1.4396	2.4810	11.0093
8	3.0	Interfant-06	F	(1.2)	71	8.2271	4.9521	5.1072	-0.4361	4.2495	4.9163
9	3.0	Interfant-06	M	(2.5)	85	8.0114	4.5490	3.3648	-0.8208	2.8412	4.5976
10	6.0	Interfant-06	F	9.5 (10.7)	98	12.3136	8.2192	8.1777	8.7455	8.1889	5.0818
11	0.1	/	F	/	96	11.2989	11.8824	9.8611	10.2911	9.2719	8.6964
12	1.0	/	M	/	98	11.6236	11.8944	8.6850	9.7199	9.8527	12.3443
13	12.0	/	F	/	90	9.1826	4.9885	1.9742	3.1891	-0.3517	2.2824
14	4.0	/	F	/	n/a	11.4695	6.3329	3.2521	4.4310	1.3435	11.4825
15	2.0	Interfant-06	M	6.0 (6.0)	90	13.3440	4.6279	2.6102	4.9218	1.1705	4.6973
16	5.5	Interfant-06	M	9.5 (15.0)	94	9.5330	9.9035	5.8136	6.3955	4.2272	6.2129
17	1.5	Interfant-06	F	10.0 (13.0)	92	6.2132	11.4431	8.3688	8.4548	6.1221	6.0703
18	3.0	Interfant-06	F	6.0 (11.5)	87	9.4723	9.2393	7.5200	8.7426	4.7647	2.0906
19	2.0	Interfant-06	F	10.5 (19)	96	7.2056	2.4819	2.0453	-1.9534	2.4821	7.8537
20	1.5	Interfant-06	M	26.5 (41.0)	96	11.2026	5.8739	4.8320	0.2568	6.2901	4.4627
21	6.5	Interfant-06	M	24.0 (32.8)	43	8.7817	6.5124	3.1900	0.3659	3.1614	11.2673
22	6.0	Interfant-06	F	19.5 (23.5)	94	10.0553	6.4983	2.9073	-1.3699	3.5784	11.5891
23	12.0	Interfant-06	F	32.0 (60.6)	92	8.0600	6.9642	4.0856	3.3604	1.6443	11.1226
24	9.0	Interfant-06	M	(84.9)	93	7.0569	3.3029	1.1508	2.1274	1.1842	8.7665
25	2.0	Interfant-06	F	(118.8)	93	10.2925	4.4468	1.7712	2.0883	0.4488	4.6017
26	3.0	Interfant-06	M	8.0 (108.5)	96	8.7375	7.0230	3.4687	4.0864	2.6431	13.0872
27	5.5	Interfant-06	M	(9.0)	95	9.1105	5.8320	2.9365	4.0461	1.5317	5.9626
28	5.0	Interfant-06	M	17.0 (33.0)	97	5.0456	5.0784	2.0327	4.8259	1.2226	5.9922
29	2.0	Interfant-06	F	56.0 (58.6)	90	9.3271	3.7605	3.9045	2.4719	4.2582	5.3297
30	1.5	Interfant-06	F	(146.1)	88	9.8910	3.3500	2.1610	0.6500	2.7175	5.8358
31	8.3	Interfant-06	F	(109.3)	81	6.5075	1.0567	0.0773	-0.7910	1.6433	2.2195
32	8.2	Interfant-06	M	(95.9)	92	7.2074	1.7896	2.8559	0.3826	0.8519	1.7726
33	10.7	Interfant-06	M	8.8 (8.8)	85	2.4138	-2.0719	0.3777	-0.1263	1.5011	2.6953
34	1.7	Interfant-06	F	(91.5)	93	6.2540	1.4646	1.9100	1.0432	2.1243	3.8579
35	11.7	Interfant-06	F	(73.2)	95	10.9273	4.7296	1.2813	3.3225	2.8393	2.9311
36	10.4	Interfant-06	F	(75.9)	92	10.4144	4.0039	2.3851	3.3520	2.9626	5.7541
37	2.4	Interfant-06	F	(73.8)	95	9.8438	5.2626	2.1926	4.1514	3.4033	13.3331
38	4.5	Interfant-06	M	16.1 (63.5)	87	11.4891	4.6039	1.4411	3.5708	2.5554	4.6562
39	1.1	Interfant-06	F	3.3 (15.7)	93	11.9464	6.0799	2.8532	4.2890	4.2377	12.9071
40	5.3	Interfant-06	M	(58.7)	94	10.3705	4.6305	2.2531	3.8496	3.0655	5.4284

Table 1. continued

Patient no.	Patient age [months]	Treatment protocol	sex	Time to event (last follow-up) [months]	% blasts	EGR3 $\Delta C_T$ Mean	IGHM $\Delta C_T$ Mean	CD79A $\Delta C_T$ Mean	BLK $\Delta C_T$ Mean	PTPN6 $\Delta C_T$ Mean	HOXA9 $\Delta C_T$ Mean
41	6.9	Infant-06	F	(63.2)	16	9.7053	5.4245	1.3355	3.4142	5.0462	9.2472
42	5.3	Infant-06	M	(60.7)	88	9.5640	3.2046	-0.1283	2.8862	1.5220	3.4737
43	0.6	Infant-06	F	5.0 (11.9)	97	8.6364	5.2214	1.5813	3.6253	2.8227	7.9122
44	1.5	Infant-06	M	17.3 (18.3)	98	9.5745	6.0122	0.6954	3.0358	3.6119	8.1333
45	4.4	Infant-06	M	6.6 (10.8)	82	10.2528	4.5355	0.2110	3.4874	2.4696	4.2993
46	9.1	Infant-06	F	39.7 (45.2)	71	9.3985	5.1434	1.5751	4.8219	2.9164	3.1663
47	0.5	Infant-06	F	8.7 (13.3)	93	9.9358	10.9029	7.9047	7.4532	8.7790	6.2701
48	6.1	AIEOP-BFM ALL 2017	F	6.6	n/a	9.4741	11.2982	8.5621	6.0722	10.3424	12.6734
49	6.1	AIEOP-BFM ALL 2017	F	8.3	n/a	10.5529	11.9934	8.9069	9.1727	8.9088	4.5847
50	10.6	/	M	/	n/a	5.1199	10.1187	9.3696	7.7286	11.0893	5.0774

Samples were taken from PB at the day of diagnosis. Gene expression values are indicated as the  $\Delta C_T$  mean of technical triplicates. % blasts Blast percentages measured at diagnosis in PB, F female, M male.

upregulated upon EGR3 overexpression ( $\log_2fc = 8.91$ ,  $p = 5.03 \times 10^{-16}$ ). In summary, GSEA identified genes involved in BCR signaling as important targets of the EGR3 induced transcriptional profile.

We assessed the surface expression of CD19 and CD79A in SEM::EGR3 and SEM::mock using flow cytometry, as the genes encoding these surface receptors were highly ranked and part of the core enrichment of the Reactome BCR signaling gene set (Fig. 2A). Remarkably, although the SEM cell line is per se CD19<sup>+</sup>, EGR3 overexpression resulted in an approximately ten-fold increase of the CD19 median fluorescence intensity (MFI) of the single cell population ( $p < 0.0001$ ) (Fig. 2B, C). Furthermore, we observed a significant relative expansion of the CD19<sup>hi</sup>CD79A<sup>+</sup> population of SEM::EGR3 ( $p = 0.0006$ ) (Fig. 2D). This expansion of phenotypic B cells (CD19<sup>hi</sup>CD79A<sup>+</sup>) was characterized by a significant increase of the CD79A MFI compared to SEM::mock ( $p = 0.0008$ ) (Fig. 2E).

These results demonstrate that upregulation of CD19 and CD79A by EGR3 led to an increase of the receptors' surface expressions. EGR3 overexpression induced B-lineage specification indicated by relative expansion of phenotypic B cells, thereby enabling functional BCR signaling as indicated by GSEA.

### EGR3 and downstream intermediate factors transactivate B-lineage specification and commitment genes

To explore the EGR3 regulome in detail, we performed binding and expression target analysis using the open source application BETA plus [24]. The BETA software algorithm integrates transcription factor ChIP-Seq data with differential gene expression data to deduce direct target genes, and is a standard processing pipeline for transcription factor binding studies [24, 32].

BETA enabled integration of MACE-Seq transcriptome data with EGR3 chromatin immunoprecipitation DNA-sequencing (ChIP-Seq) data of SEM::EGR3 and SEM::mock. ChIP-Seq data were already obtained during our former study (GSE205652).

The BETA algorithm ranked genes according to the regulatory potential score and assigned to the cumulative percentage of genes. Plotting this assignment as a graph visualized that EGR3 owns a direct activating and repressive function, and thus, acts as a direct transactivator and -repressor in *KMT2A::AFF1* proB-ALL (Fig. 3A).

In total, 3890 directly upregulated and 3107 downregulated EGR3 target genes were identified, referred to as the EGR3 regulome. We used the PANTHER classification system [25] to functionally characterize the EGR3 regulome. This analysis revealed that EGR3 transactivates and -represses the same classes of genes (Fig. 3B), involved in the same biological functions (Fig. 3C) and located on the same chromosomes (Fig. 3D). Especially the class 'gene-specific transcriptional regulator' comprised more directly activated ( $n = 361$ ) than repressed ( $n = 212$ ) genes. Concordant with this, a higher number of transactivated ( $n = 1229$ ) than -repressed ( $n = 840$ ) genes were related to the Gene Ontology (GO) term 'biological regulation' (Fig. 3C).

We compared the BCR pathway-related genes of the EGR3 transcriptome with those of the regulome (Fig. 3E, F) and identified 64 of 114 genes (56.1%) as direct EGR3 targets, including CD79A, BLK, PTPN6, CD19, and CD22 (Table 6). Thus, the remaining 50 genes including IGHM were indirect EGR3 targets and transactivated by unknown intermediate transcription factors. To uncover these transcription factors, a motif analysis of all differentially expressed genes (MACE-Seq data) and all direct EGR3 targets (ChIP-Seq data) was performed using BETA plus. As expected, the highest scoring and significant consensus sequence found in all up- and downregulated target genes matched that one of EGR3 and other transcription factors binding to the same or a highly similar motif including EGR1, EGR2, EGR4, KLF16, SP3, and

**Table 2.** Patient characteristics of the rel cohort ( $n = 18$ ).

Patient no.	Age at primary diagnosis [months]	KMT2A-r partner	sex	EGR3 $\Delta C_T$ Mean	IGHM $\Delta C_T$ Mean	CD79A $\Delta C_T$ Mean	BLK $\Delta C_T$ Mean	PTPN6 $\Delta C_T$ Mean
REZ1	1.3	AFF1	F	2.8330	3.6274	2.5294	6.2860	4.2386
REZ2	2.9	MLLT1	M	4.1774	8.3719	6.2586	7.3628	4.5660
REZ3	3.8	AFF1	F	4.3014	11.1143	7.5835	9.1950	10.0947
REZ4	2.5	AFF1	F	6.6574	12.0503	10.1751	11.9828	9.3876
REZ5	1.2	AFF1	F	1.1889	10.5701	8.1192	9.9020	9.5213
REZ6	10.7	MLLT1	M	5.1781	5.0754	3.5868	-0.4993	3.8987
REZ7	4.3	MLLT1	M	3.7298	6.0183	5.0341	-0.4709	6.2223
REZ8	3.6	MLLT3	F	4.7424	3.6338	4.7103	0.1660	3.3973
REZ9	9.1	AFF1	F	2.2762	10.9410	7.9419	8.6553	9.9990
REZ10	0.7	AFF1	F	1.6308	13.4663	9.1956	10.7877	10.0112
REZ11	4.4	AFF1	M	6.5653	10.6022	9.1016	10.0768	11.0481
REZ12	4.2	AFF1	M	5.0302	5.1254	3.0619	4.9896	1.7865
REZ13	2.0	AFF1	F	2.5849	7.4593	4.5334	4.2896	1.5519
REZ14	3.1	AFF1	F	8.4397	10.9710	7.2141	9.6779	1.5646
REZ15	7.6	AFF1	F	7.8336	4.8100	5.3276	6.5240	4.4725
REZ16	6.7	AFF1	M	9.5416	9.4965	5.6740	8.0000	4.4870
REZ17	5.3	AFF1	M	9.8667	5.2598	3.3857	-0.1229	5.3876
REZ18	7.2	AFF1	M	6.7247	5.9524	3.2850	0.2192	4.3320

Samples were taken from PB at relapse diagnosis. Gene expression values are indicated as the  $\Delta C_T$  mean of technical triplicates. F female, M male.

**Table 3.** Oligonucleotides used in this study.

Name	Sequence (5' -> 3')	Application
GAPDH_fwd	TTGCCCTCAACGACCACTTT	qRT-PCR
GAPDH_rev	TGGTCCAGGGGTCTTACTCC	qRT-PCR
IGHM_fwd	CATCTGACCGTGTCCGAAG	qRT-PCR
IGHM_rev	TGGCCACAGGTTCTCAAAG	qRT-PCR
CD79A_fwd	ACCGAATCATCACAGCCGAG	qRT-PCR
CD79A_rev	CAACCCGAGCTTCTCGTTCT	qRT-PCR
BLK_fwd	GACAGTGAATACACGGCCCA	qRT-PCR
BLK_rev	CCCGCCATAAGTGACAACCT	qRT-PCR
PTPN6_fwd	GAGGCGCAGTACAAGTTCATC	qRT-PCR
PTPN6_rev	GTTCCCGTACTCCGACTCCT	qRT-PCR

SP8 (Fig. 4A). Lower scoring binding motifs of up- and down-regulated genes were assigned to ZEB1, ZNF354C, and SOX10, indicating potential alternate regulation of EGR3 target genes by these transcription factors. Scanning for enriched motifs in differentially expressed but not direct EGR3-regulated genes identified a set of motif-assigned transcription factors. Of these were *GATA3*, *FOXO6*, and *E2F1* strongly upregulated direct EGR3 targets, and *PAX5* an indirect EGR3 target with strong differential expression ( $\log_2fc = 9.47$ ,  $p = 4.95 \times 10^{-41}$ ) (Fig. 4B). Especially *PAX5* has been described as a mediator of B cell identity and B-lineage commitment [33–35]. Furthermore, analysis of the Leukemia MILE study data set using BloodSpot revealed the strongest gene correlations of *PAX5* to be *CD19* and *CD79A*. Concluding this, the binding and expression target analysis followed by motif scanning uncovered *GATA3*, *FOXO6*, *E2F1*, and *PAX5* as intermediate factors in the EGR3 transcriptomic

**Table 4.** Antibodies used in this study.

Antibody	Source	Identifier
PE Mouse Anti-Human CD79a Monoclonal Antibody	BD	BD Biosciences Cat# 563777, RRID: AB_2738423
BV421 Mouse Anti-Human IgM Monoclonal Antibody	BD	BD Biosciences Cat# 562618, RRID: AB_2737681
APC-H7 Mouse Anti-Human CD19 Monoclonal Antibody	BD	BD Biosciences Cat# 560177, RRID: AB_1645470

network, regulating B-lineage specification and commitment gene expression.

#### **IGHM, CD79A, BLK and PTPN6 expressions correlate strongly with each other and partly with EGR3 among 50 infant KMT2A::AFF1 proB-ALL patients**

We aimed to investigate the regulation of B-lineage specification and commitment gene expression by EGR3 in patient material and therefore assessed the transcription levels of *IGHM*, *CD79A*, *BLK*, and *PTPN6* in 50 infant *KMT2A::AFF1* proB-ALL patients at diagnosis (Table 1). This patient cohort was already investigated in our recent study [5], from which we obtained the *EGR3* expressions. cDNA of peripheral blood was used for quantitative real-time PCR (qRT-PCR) based gene expression measurement and subsequent Pearson correlation testing of  $\Delta C_T$  values was performed. The resulting Pearson correlation matrix demonstrated a very strong and highly significant correlation between the *IGHM*, *CD79A*, *BLK*, and *PTPN6* gene expressions with Pearson  $r$  values above 0.70, suggesting their collective belonging to a distinct gene expression program (Fig. 5A, B).

**Table 5.** Top fifty gene sets enriched in phenotype EGR3.

rank	gene set	size	ES	NES	FDR q-val	rank at max
1	REACTOME_SIGNALING_BY_THE_B_CELL_RECEPTOR_BCR	114	0.41	2.96	0.05	4040
2	LI_WILMS_TUMOR_VS_FETAL_KIDNEY_1_DN	164	0.41	2.79	0.05	1819
3	GNF2_PTPRC	67	0.62	2.74	0.05	2657
4	WP_B_CELL_RECEPTOR_SIGNALING_PATHWAY	97	0.55	2.73	0.05	3716
5	GOBP_POSITIVE_REGULATION_OF_INTERFERON_BETA_PRODUCTION	37	0.52	2.73	0.05	2366
6	GOBP_ATP_METABOLIC_PROCESS	201	0.38	2.71	0.05	4185
7	HP_MYOCLOONUS	348	0.42	2.71	0.05	4350
8	YAP1_UP	43	0.51	2.7	0.05	4532
9	GOBP_INTERFERON_BETA_PRODUCTION	55	0.51	2.67	0.05	2366
10	REACTOME_DDX58_IFIH1_MEDIATED_INDUCION_OF_INTERFERON_ALPHA_BETA	68	0.46	2.66	0.05	2201
11	ALCALA_APOPTOSIS	85	0.41	2.66	0.05	2052
12	DER_IFN_BETA_RESPONSE_UP	103	0.43	2.66	0.05	3809
13	BROWNE_INTERFERON_RESPONSIVE_GENES	64	0.57	2.66	0.05	3071
14	GNF2_VAV1	35	0.58	2.66	0.05	3195
15	HP_BRITTLE_HAIR	40	0.52	2.65	0.05	1355
16	GOBP_DEFENSE_RESPONSE_TO_SYMBIONT	257	0.43	2.63	0.05	3422
17	NGUYEN_NOTCH1_TARGETS_DN	82	0.5	2.62	0.05	3342
18	PID_BCR_5PATHWAY	63	0.54	2.61	0.05	3716
19	HP_CHOREOATHETOSIS	99	0.41	2.61	0.05	3007
20	REACTOME_SARS_COV_INFECTIONS	355	0.34	2.61	0.05	6457
21	HP_MEMORY_IMPAIRMENT	139	0.43	2.61	0.05	3896
22	GOBP_RESPONSE_TO_VIRUS	347	0.44	2.59	0.05	3494
23	HALLMARK_INTERFERON_ALPHA_RESPONSE	96	0.46	2.56	0.05	4121
24	GOBP_REGULATION_OF_INTRACELLULAR_TRANSPORT	320	0.35	2.56	0.05	6271
25	HP_NEOPLASM_OF_THE_LIVER	124	0.49	2.55	0.05	5154
26	WP_APOPTOSIS	85	0.46	2.55	0.05	3921
27	REACTOME_TAK1_DEPENDENT_IKK_AND_NF_KAPPA_B_ACTIVATION	43	0.53	2.54	0.05	2041
28	HP_ECTOPIC_CALCIFICATION	209	0.44	2.54	0.05	3466
29	HP_ABNORMAL_CNS_MYELINATION	307	0.36	2.53	0.05	6718
30	BOQUEST_STEM_CELL_DN	206	0.51	2.52	0.05	2711
31	HP_WEAKNESS_DUE_TO_UPPER_MOTOR_NEURON_DYSFUNCTION	469	0.39	2.52	0.05	4528
32	HP_ACUTE_LEUKEMIA	105	0.41	2.52	0.05	5158
33	REACTOME_RHO_GTPASE_CYCLE	436	0.37	2.52	0.05	4897
34	HOEBEKE_LYMPHOID_STEM_CELL_UP	92	0.44	2.51	0.05	2556
35	GOBP_REGULATION_OF_VIRAL_GENOME_REPLICATION	82	0.45	2.51	0.05	3466
36	REACTOME_INTERLEUKIN_1_FAMILY_SIGNALING	144	0.39	2.51	0.05	2041
37	REACTOME_CYTOSOLIC_SENSORS_OF_PATHOGEN_ASSOCIATED_DNA	62	0.41	2.51	0.05	2201
38	WANG_TARGETS_OF_MLL_CBP_FUSION_UP	43	0.49	2.51	0.05	4346
39	GYORFFY_DOXORUBICIN_RESISTANCE	33	0.65	2.51	0.05	2036
40	HALLMARK_ALLOGRAFT_REJECTION	179	0.55	2.51	0.05	3064
41	GOBP_ACTIVATION_OF_GTPASE_ACTIVITY	109	0.49	2.51	0.05	2641
42	GNF2_MYD88	59	0.5	2.49	0.05	2926
43	MODULE_256	58	0.46	2.49	0.05	4870
44	HP_CHRONIC_DIARRHEA	75	0.48	2.48	0.05	3992
45	HP_ABNORMALITY_OF_CARDIOVASCULAR_SYSTEM_ELECTROPHYSIOLOGY	449	0.4	2.48	0.05	3898
46	YAGI_AML_WITH_T_8_21_TRANSLOCATION	351	0.39	2.48	0.05	5568
47	HP_PREMATURE_GRAYING_OF_HAIR	39	0.51	2.48	0.05	1796
48	HP_CNS_DEMYELINATION	39	0.61	2.48	0.05	4378
49	HP_SHORTENING_OF_ALL_DISTAL_PHALANGES_OF_THE_FINGERS	39	0.52	2.48	0.05	5023
50	GOBP_REGULATION_OF_GENERATION_OF_PRECURSOR_METABOLITES_AND_ENERGY	122	0.45	2.48	0.05	4933

ES enrichment score, NES nominal ES, FDR false discovery rate.



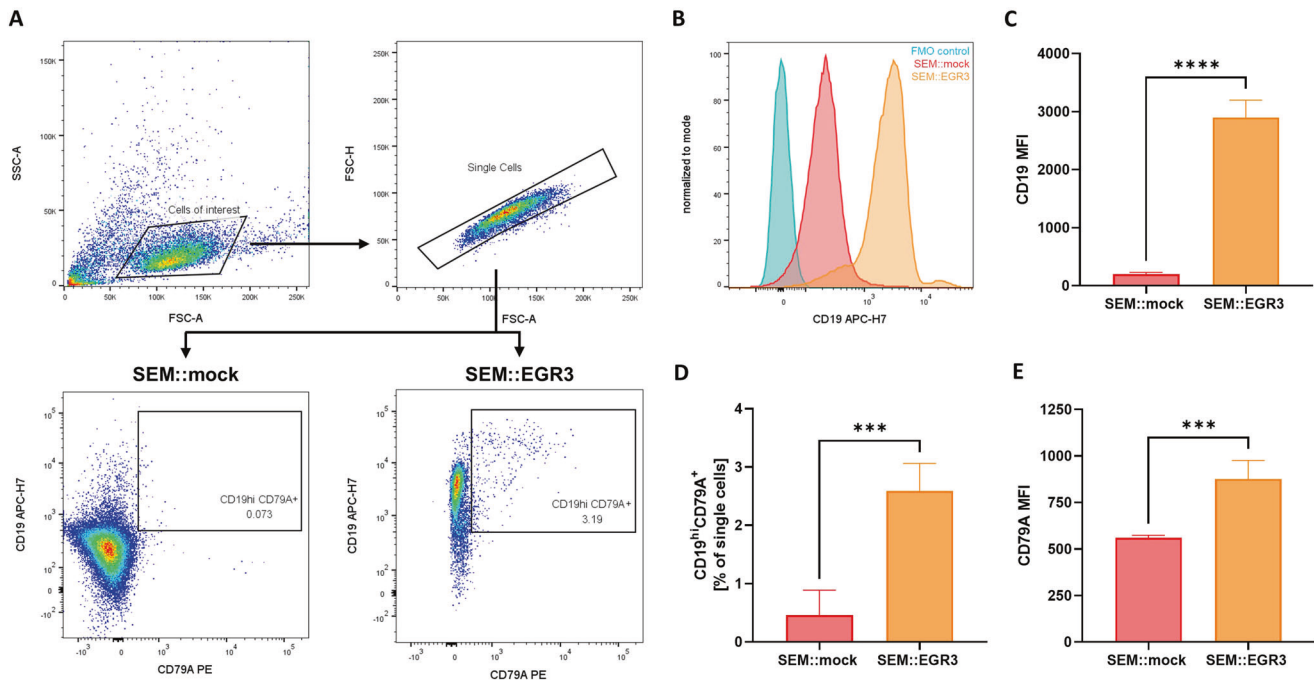


**Fig. 2** Flow cytometric analysis of SEM::EGR3 and SEM::mock. **A** Gating strategy. Single cells were gated out of cells of interest for assessment of CD19 and CD79A surface expressions. Analyses were performed based on four biological replicates. **B** Exemplary histogram of CD19 fluorescence intensities of a full-fluorescence-minus-anti CD19 (FMO) control (blue), SEM::mock (red) and SEM::EGR3 (orange). Plots display the respective single cell populations and were normalized to mode. **C** CD19 median fluorescence intensities (MFI) of SEM::mock and SEM::EGR3 singlets. Significance was tested using a two-tailed *t* test ( $p < 0.0001$ ). Error bars indicate standard deviation. **D** Mean percentages of the CD19<sup>hi</sup>CD79A<sup>+</sup> population relative to singlets. Error bars indicate standard deviation and significance was tested using a two-tailed *t* test ( $p = 0.0006$ ). **E** CD79A median fluorescence intensities (MFI) of the CD19<sup>hi</sup>CD79A<sup>+</sup> populations of SEM::mock and SEM::EGR3. Significance was tested using a two-tailed *t* test ( $p = 0.0008$ ). Error bars indicate standard deviation.

The transcription levels of *EGR3* correlated less strongly with *IGHM* and *BLK* (Pearson  $r = 0.35$  and  $0.34$ , respectively) (Fig. 5C–G), and not significantly with *CD79A* and *PTPN6* (Fig. 5C, H–K). Apart from that, higher patient age correlated with higher *EGR3* expression (Pearson  $r = -0.31$ ), whereas this was not the case for *IGHM*, *CD79A*, *BLK*, and *PTPN6* (Fig. 5L).

These results confirm the B-lineage phenotype associated with engineered *EGR3*-overexpression suggesting direct causality between *EGR3* expression and B-lineage specification. Furthermore, other factors are likely to influence the *EGR3* target gene expression as well. The latter conclusion is concordant with the motif scan revealing that *EGR1*, *EGR2*, *EGR4*, *KLF16*, *SP3*, *SP8*, *ZEB1*, *ZNF354C*, and *SOX10* bind the same genes as *EGR3*, suggesting these factors as possible co-regulators.

#### Low *IGHM*, *CD79A*, *BLK*, and *PTPN6* expressions indicate a patient subgroup with inferior EFS

The strong correlation between the *IGHM*, *CD79A*, *BLK*, and *PTPN6* gene expressions prompted us to analyze their distribution within the patient cohort. For that purpose, a principal component analysis (PCA) of the expression levels was conducted using the open-source tool ClustVis [22], uncovering a distinct bimodal distribution of patient clusters (Fig. 6A). The corresponding heatmap visualized that patients showed either a high (BCR<sup>hi</sup>,  $n = 37$ ) or low (BCR<sup>lo</sup>,  $n = 13$ ) expression of the analyzed B-lineage-related genes (Fig. 6B). This bimodal distribution points to differences in the B-lineage specification process, with BCR<sup>lo</sup> patients having a less committed B cell identity, indicated by the low expression of B-lineage-representing genes. Accordingly, the high expression of *IGHM*,

*CD79A*, *BLK*, and *PTPN6* in the BCR<sup>hi</sup> group indicates a more mature proB-cell phenotype. The strict bimodal clustering suggests that the development from BCR<sup>lo</sup> to BCR<sup>hi</sup> is rather a stepwise maturation process than a fluent transition, and presumably reflects the developmental stages of early and late proB cells.

We compared the event-free survival (EFS) for all patients with available outcome data ( $n = 43$ ) considering their assignment to the BCR<sup>lo</sup> ( $n = 9$ ) or BCR<sup>hi</sup> ( $n = 34$ ) group. Four-year-EFS of BCR<sup>lo</sup> patients was significantly poorer, reaching only  $22.2 \pm 13.9\%$  compared to  $49.8 \pm 9.3\%$  of the BCR<sup>hi</sup> group ( $p = 0.0205$ , Fig. 6C). Notably, all events within the BCR<sup>lo</sup> group occurred within the first 12 months from diagnosis. To test for age and *HOXA9* status as possible confounders, we performed the same PCA analysis with patients assigned to age groups (0–6 months vs. 6–12 months) (Fig. 6D, E) and to *HOXA9* status groups (*HOXA9* high vs. low) (Fig. 6F, G). We observed that both factors did not affect dichotomous separation of patients as young and old as well as *HOXA9* high and low groups overlap almost completely.

#### BCR<sup>lo</sup> vs. BCR<sup>hi</sup> clustering of patients is sustained at relapse

Considering the elevated level of *EGR3* expression at relapse in infant *KMT2A-r* proB-ALL, we aimed to examine the *IGHM*, *CD79A*, *BLK*, and *PTPN6* gene expressions at the time of relapse. To do so, we performed the same gene expression analysis with the relapse (rel) cohort of our former study. This cohort comprised 18 infant *KMT2A-r* proB-ALL patients (14 *KMT2A::AFF1* cases) at the time of relapse, composing an independent cohort, not matched to the diagnosis (dx) cohort (Table 2).

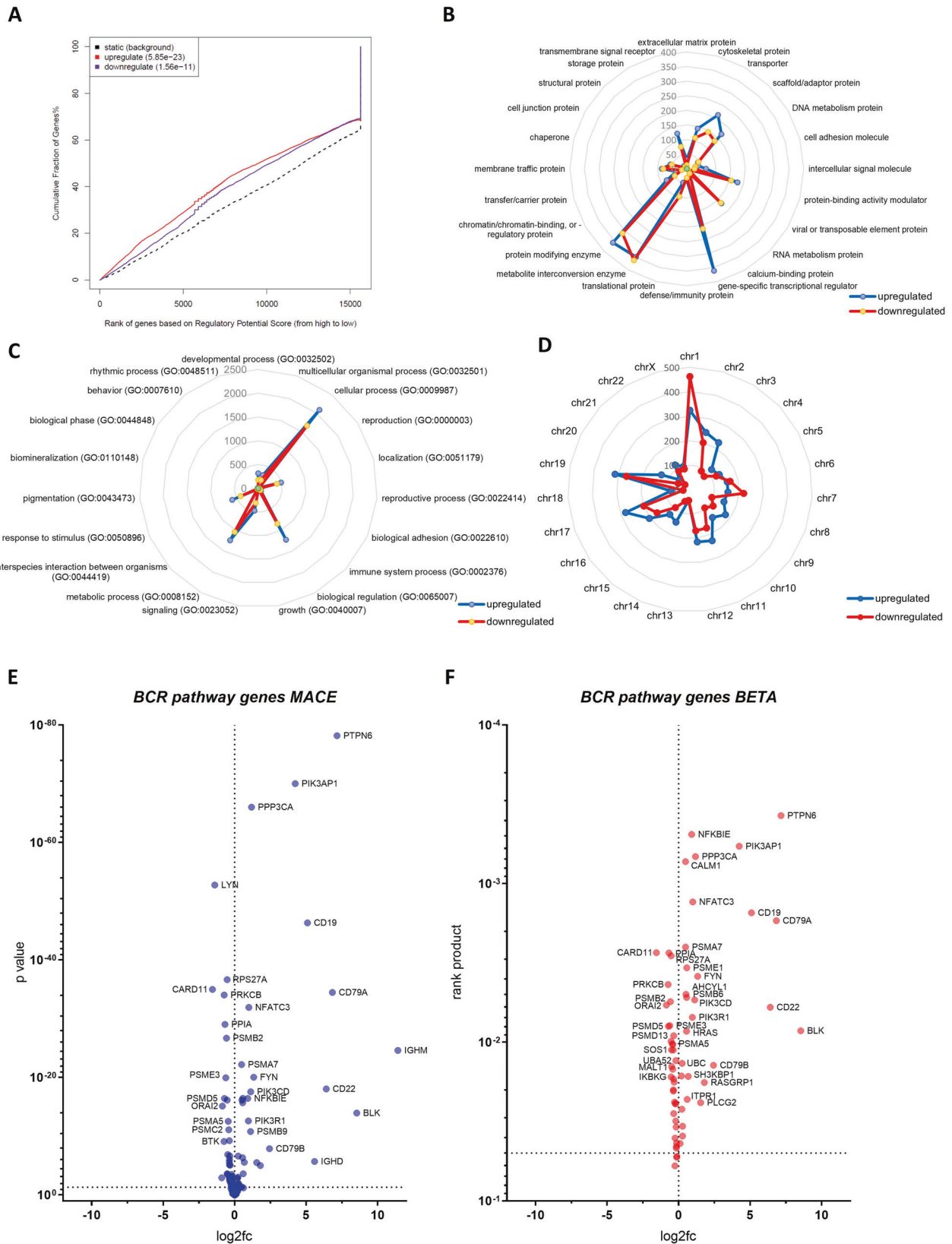


**Fig. 3** Integration of MACE-Seq and ChIP-Seq data revealed the EGR3 regulome of infant *KMT2A::AFF1* ALL. **A** Assignment of gene ranks to the cumulative fraction of genes using BETA identifies EGR3 as a direct activator and repressor of target genes. Analysis of the EGR3 regulome using the PANTHER database with up- and downregulated target genes subclassified considering their corresponding protein class (**B**), biological function/GO term (**C**) and chromosomal location (**D**). Numbers indicate the count of up- (blue) and downregulated (red) genes. **E** Volcano plot visualizing genes of the Reactome BCR geneset according to their differential expression indicated as the log<sub>2</sub>-fold change (log<sub>2</sub>fc) and *p* value (MACE-Seq data). **F** Volcano plot visualizing genes of the Reactome BCR geneset according to their differential expression (log<sub>2</sub>fc) and direct EGR3 regulation (rank product) (MACE-Seq and BETA data).

**Table 6.** Genes of the set ‘signaling by the B cell receptor’ (Reactome, R-HSA-983705), their type of regulation by EGR3 and differential expression.

gene	direct EGR3 target?	log2fc MACE-Seq	p value MACE-Seq	rp BETA
<i>IGHM</i>	no	11.42362217	2.48921E-25	n/a
<i>BLK</i>	yes	8.55098816	1.10908E-14	8.46E-03
<i>PTPN6</i>	yes	7.164737984	6.50833E-79	0.0003723
<i>CD79A</i>	yes	6.842767882	3.2689E-35	0.001712
<i>CD22</i>	yes	6.416448966	8.85632E-19	0.006018
<i>IGHD</i>	no	5.59443973	1.92888E-06	n/a
<i>CD19</i>	yes	5.097472391	4.62783E-47	0.001527
<i>PIK3AP1</i>	yes	4.246158952	9.22432E-71	0.0005812
<i>CD79B</i>	yes	2.440657291	1.33431E-08	0.01395
<i>RASGRP1</i>	yes	1.805660433	9.81104E-06	0.01795
<i>PLCG2</i>	yes	1.549262561	3.06887E-06	0.02405
<i>FYN</i>	yes	1.335261599	8.88319E-21	0.00384
<i>PPP3CA</i>	yes	1.184342322	9.44927E-67	0.0006748
<i>PIK3CD</i>	yes	1.124084067	2.75855E-18	0.005402
<i>PSMB9</i>	no	1.120899683	1.59578E-11	n/a
<i>NFATC3</i>	yes	0.998713529	1.18837E-32	0.001304
<i>PIK3R1</i>	yes	0.966311084	2.44716E-13	0.006969
<i>NFKBIE</i>	yes	0.914332634	3.75272E-17	0.0004891
<i>SH3KBP1</i>	yes	0.677658035	2.64864E-06	0.01642
<i>PSMA6</i>	no	0.628450298	0.062177736	n/a
<i>ITPR1</i>	yes	0.608990433	0.000233393	0.02294
<i>PSME1</i>	yes	0.579774438	3.5101E-17	0.003389
<i>PSMB6</i>	yes	0.565638656	2.03686E-16	0.005221
<i>HRAS</i>	yes	0.553028624	4.35293E-07	0.008516
<i>AHCYL1</i>	yes	0.516916343	6.89158E-17	0.004982
<i>CALM1</i>	yes	0.491872592	0.039246507	0.000727
<i>PSMA7</i>	yes	0.491383232	6.26317E-23	0.002513
<i>DAPP1</i>	no	0.388597531	0.052583747	n/a
<i>FBXW11</i>	yes	0.285022076	0.011951906	0.03383
<i>PPP3CB</i>	yes	0.27924157	0.031691017	0.03899
<i>UBC</i>	yes	0.253791938	2.26985E-07	0.01359
<i>PSMB8</i>	no	0.250209285	0.011026312	n/a
<i>PPP3R1</i>	yes	0.229316482	0.000922238	0.02644
<i>PSMC1</i>	no	0.223758639	0.21214738	n/a
<i>PSMD8</i>	yes	0.206878775	0.001486499	0.01632
<i>NCK1</i>	no	0.177428109	0.185595712	n/a
<i>KRAS</i>	no	0.137742679	0.142867744	n/a
<i>PSMA8</i>	no	0.12351416	0.636113579	n/a
<i>FKBP1A</i>	yes	0.113168534	0.057549916	0.04344
<i>PSME2</i>	no	0.109161404	0.272267991	n/a
<i>PSMD6</i>	no	0.099468329	0.227417909	n/a
<i>BCL10</i>	no	0.097846109	0.427668399	n/a
<i>PSMB3</i>	no	0.093466114	0.130863049	n/a
<i>PSMA2</i>	no	0.092612935	0.73577585	n/a
<i>PSMB11</i>	no	0.092497922	0.727664144	n/a
<i>PSMB10</i>	no	0.091210982	0.717981181	n/a
<i>PSMB7</i>	no	0.078594367	0.197210636	n/a
<i>UBB</i>	no	0.077804248	0.077068512	n/a
<i>PSMC6</i>	no	0.07662523	0.396738012	n/a
<i>MAP3K7</i>	no	0.053871719	0.520389098	n/a
<i>NFATC1</i>	no	0.017988661	0.842017304	n/a

Table 6. continued

gene	direct EGR3 target?	log2fc MACE-Seq	p value MACE-Seq	rp BETA
BLNK	no	0.012076394	0.962179165	n/a
IGLC3	no	0.005188884	0.98330526	n/a
PSMC5	no	0.002298519	0.966883202	n/a
IGLC2	no	0	1	n/a
PSMD2	no	-0.000438565	0.99385484	n/a
PSMC3	no	-0.009374859	0.871548561	n/a
SEM1	no	-0.035848586	0.536641158	n/a
BTRC	no	-0.043122119	0.743614989	n/a
NFKBIB	no	-0.048602913	0.641683594	n/a
ORAI1	no	-0.050325263	0.689236497	n/a
ITPR2	no	-0.057315013	0.696661836	n/a
NRAS	no	-0.067952655	0.403682448	n/a
PSMC4	no	-0.090473401	0.188421226	n/a
CHUK	no	-0.09213649	0.463552091	n/a
PSMD14	no	-0.099389355	0.149921007	n/a
REL	no	-0.105755893	0.567292607	n/a
PSMB5	yes	-0.117300018	0.071947041	0.0525
PSMA3	yes	-0.12765023	0.056413726	0.05304
PSMA4	no	-0.12765023	0.056413726	n/a
STIM1	no	-0.13504264	0.135062364	n/a
PSMD4	yes	-0.136908983	0.043599216	0.04312
TRPC1	no	-0.140211415	0.566506534	n/a
PSMB4	yes	-0.143316292	0.008444496	0.04541
SKP1	yes	-0.155405082	0.007980788	0.04654
NFATC2	no	-0.16313576	0.21867056	n/a
SYK	no	-0.163962068	0.061590912	n/a
PSMD3	yes	-0.170338294	0.002588761	0.03421
UBA52	yes	-0.18111628	0.000640896	0.01305
PSMD10	no	-0.182449259	0.046626892	n/a
PSMB1	yes	-0.191173577	0.000313825	0.03138
PSMD7	yes	-0.193336641	0.001402521	0.02428
RELA	yes	-0.219182607	0.005520858	0.02449
PSMF1	yes	-0.241001349	0.001520813	0.04021
NFKB1	no	-0.243914024	0.029935823	n/a
PSMD9	yes	-0.25415219	0.084691328	0.06018
CUL1	yes	-0.277874069	0.000645415	0.02387
NFKBIA	no	-0.284994997	0.008752111	n/a
GRB2	yes	-0.310478144	8.1543E-06	0.01782
PSMD13	yes	-0.338660552	2.25353E-07	0.009095
IKBKB	yes	-0.340568298	0.003982831	0.02814
ITPR3	yes	-0.345267237	0.002182622	0.01704
PSMD1	yes	-0.355786358	8.26092E-07	0.02033
PSME4	no	-0.356370366	7.30394E-06	n/a
PSMD12	yes	-0.369060374	2.31513E-06	0.01996
PSMA1	yes	-0.370940312	5.60831E-10	0.01119
VAV1	yes	-0.396708907	0.000758081	0.01034
PSMC2	yes	-0.406420999	8.04357E-12	0.01478
PSMA5	yes	-0.44324155	2.8338E-13	0.01024
MALT1	yes	-0.479264577	1.28722E-07	0.01421
SOS1	yes	-0.486278337	0.000293116	0.01117
PSMD11	yes	-0.517998908	7.00864E-17	0.009862

Table 6. continued

gene	direct EGR3 target?	log2fc MACE-Seq	p value MACE-Seq	rp BETA
<i>RPS27A</i>	yes	-0.518177519	2.15808E-37	0.002853
<i>IKBKG</i>	yes	-0.518676703	0.000234099	0.01656
<i>PSMB2</i>	yes	-0.565388038	2.01317E-27	0.005551
<i>PSME3</i>	yes	-0.610618137	1.09492E-20	0.007852
<i>PPIA</i>	yes	-0.673833501	9.15098E-30	0.002734
<i>PSMD5</i>	yes	-0.706954282	3.71916E-17	0.007929
<i>PRKCB</i>	yes	-0.731810409	8.84403E-35	0.004322
<i>BTK</i>	no	-0.742153419	7.76623E-10	n/a
<i>ORAI2</i>	yes	-0.847816906	7.16229E-16	0.005828
<i>RASGRP3</i>	no	-0.902579249	0.001205017	n/a
<i>LYN</i>	no	-1.383822477	1.74706E-53	n/a
<i>CARD11</i>	yes	-1.549753074	9.97827E-36	0.002724

log2fc log2 fold change, rp rank product.

As for the dx cohort, a PCA revealed co-segregation of patients into a BCR<sup>lo</sup> and a BCR<sup>hi</sup> group (Fig. 7A). Contrasting the dx cohort, clustering of relapsed patients was less cohesive, with patients REZ2, REZ14, and REZ16 exhibiting low *IGHM*, *CD79A*, and *BLK* expressions, but increased *PTPN6* gene expression levels reaching those of the BCR<sup>hi</sup> group (Fig. 7B).

Pearson correlation testing of the  $\Delta C_T$  values showed strong correlations between the *IGHM*, *CD79A*, *BLK*, and *PTPN6* gene expressions, almost resembling the Pearson r and corresponding p values of the dx cohort (Fig. 7C–H). Contrasting the dx cohort, the rel cohort did not indicate a significant correlation for any of the aforementioned gene expressions with that of *EGR3* (Fig. 7I). The transcription level of *EGR3* was approximately 100-fold elevated at relapse compared to diagnosis, independent of BCR<sup>lo</sup> or BCR<sup>hi</sup> classification (Fig. 7K). Unlike *EGR3*, the expressions of *IGHM*, *CD79A*, *BLK*, and *PTPN6* were not generally elevated at relapse, rather were the expression level differences between the BCR<sup>lo</sup> and BCR<sup>hi</sup> groups almost the same comparing the diagnosis and relapse cohorts (Fig. 7M–P). These results indicate that BCR<sup>lo</sup> vs. BCR<sup>hi</sup> clustering of patients was sustained at relapse and elevated *EGR3* levels were not concomitant with *IGHM*, *CD79A*, *BLK* and *PTPN6* gene expressions. This suggests a minor role for *EGR3* in B-lineage-specific gene regulation at the time of relapse and demonstrates preservation of both developmental proB cell stages during relapse formation, although to a lesser extent.

## DISCUSSION

This study identified *EGR3* as a regulator of B-lineage specification and commitment processes in the context of infant *KMT2A::AFF1* acute lymphoblastic leukemia. This characterization is in line with the fact that *EGR3* is generally downregulated in B cell malignancies according to the Leukemia MILE study [27] and upregulated in naïve and mature B cells referring to the Bloodspot DMAP dataset [26] (Supplementary Fig. 1B). Furthermore, the murine homologues *Egr3* and *Egr2* are required for B cell proliferation upon antigen receptor stimulation [20, 36]. Accordingly, our study and these data imply the limitation of *EGR3* expression to be concomitant with a differentiation block of the B-lineage in hematologic malignancies.

That *EGR3* is involved in B-lineage specification and commitment is further strengthened by the identification of *PAX5* as an intermediate factor of the *EGR3* regulome. *PAX5* is a known activator of B cell identity regulating the gene expression of *CD19*,

*CD79B*, and *EBF1* [33, 37]. In addition, *PAX5* is a regulator of B cell development [38] and B-lineage commitment [35, 39, 40]. In this regard, an important difference between *EGR3* and *PAX5* is that the latter not only binds DNA response elements but also regulates chromatin accessibility at target promoters [41]. This points to a collaborative effect of *EGR3* and *PAX5*, regulating in part the same genes by different means.

Finally, *CD19* is commonly accepted as a hallmark B cell commitment marker [42, 43], and we demonstrate direct transcriptional upregulation of *CD19* by *EGR3* resulting in approximately ten-fold increased surface expression of the corresponding protein (Fig. 2). Importantly, *CD19*-directed therapies including CAR T cells and Blinatumomab were reported to lead to lineage switch of infant *KMT2A::AFF1* ALL [44–46]. This process has been shown to be accompanied by a loss of the B-lineage-specific transcription factors *EBF1* and *PAX5* [47]. As our data suggest a collaborative effect between *PAX5* and *EGR3*, the role of *EGR3* during lineage switch of *KMT2A-r* B ALL needs further investigation.

In contrast to primary diagnosis, elevated *EGR3* expression at relapse was not accompanied by increased expression of B lineage-associated direct targets. Consequently, *EGR3* expression at relapse does not indicate a more committed or mature proB cell identity, but could reflect external stress stimuli including response to chemotherapy or inflammatory mediators in the leukemic microenvironment as *EGR3* is involved in rapid and transient stress responses and inflammatory signaling [48, 49].

Fetal pre-pro B cells are the earliest B-lineage-committed progenitors giving rise to proB cells [50]. In this context, both progenitor subtypes can be distinguished regarding their expression of B cell-associated genes including *CD79A*, *CD19*, *PAX5*, *MME*, *EBF1*, *DNTT* among many others [50]. As we worked with RNA extracted from peripheral blood, our gene expression analysis considered mainly the blast population. Therefore, it is very likely that clustering of patients into the BCR<sup>lo</sup> and BCR<sup>hi</sup> group at diagnosis and relapse represents an early vs. late proB state of the blast population, with BCR<sup>lo</sup> representing pre-proB cells and BCR<sup>hi</sup> proB cells. This interpretation is in line with the understanding of B-lineage commitment as a stepwise process, orchestrated by transcription factor-mediated gene regulatory networks [51, 52]. Furthermore, the inferior survival of the BCR<sup>lo</sup> group could be explained by decreased maturity of blasts within the proB cell state, likely to go along with elevated lineage plasticity, a hallmark of *KMT2A-r* leukemia and



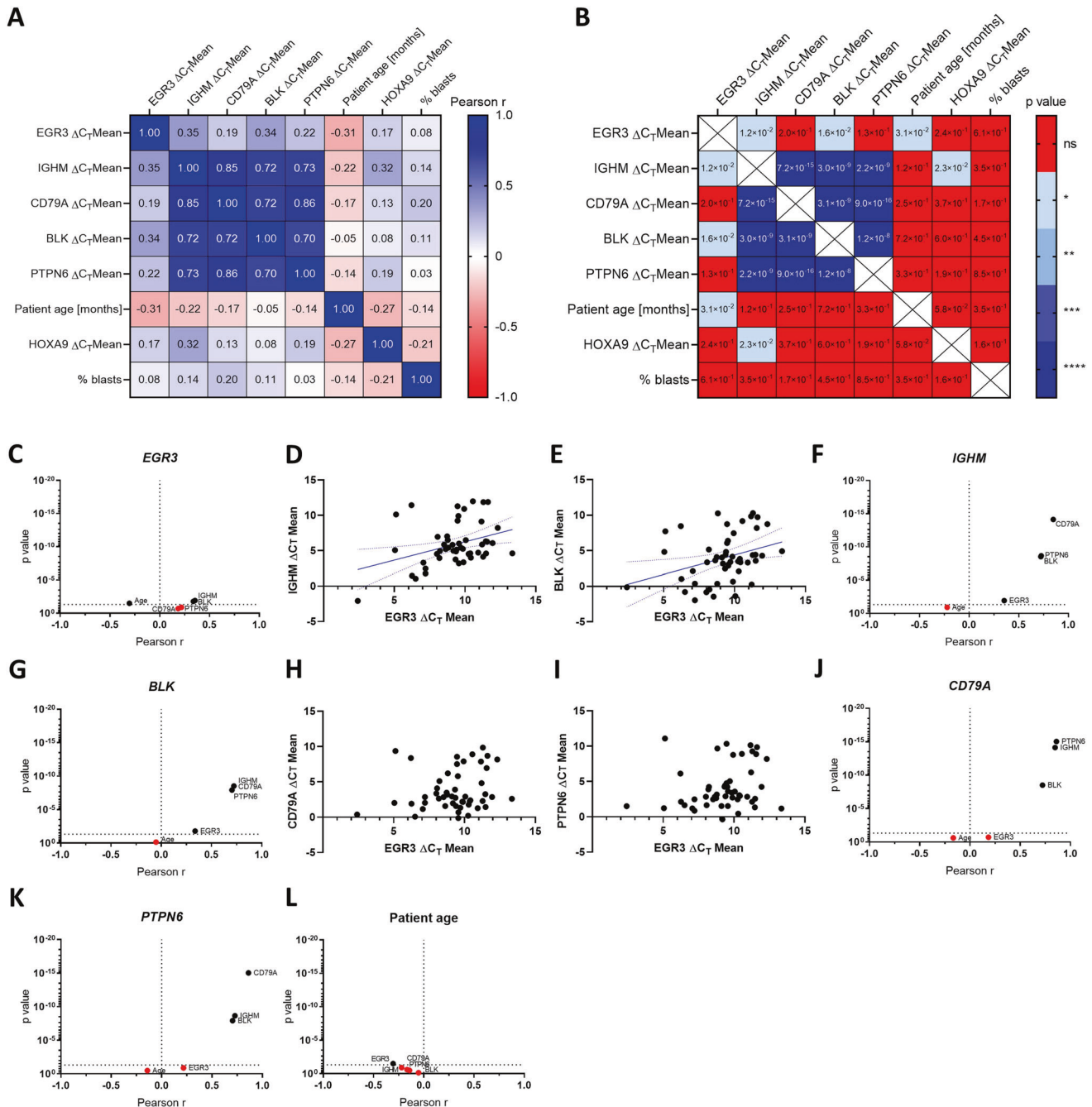


**Fig. 5** Pearson correlation testing of the diagnosis cohort. Pearson correlation matrix indicating the Pearson  $r$  value (A) and  $p$  value (B) of all tested correlations. Volcano plots showing Pearson correlations of *EGR3* (C), *IGHM* (F), *BLK* (G), *CD79A* (J), *PTPN6* (K) and patient age (L). Correlations with  $p \geq 0.05$  were considered non-significant and marked in red. Patients plotted according to their *IGHM/EGR3* (D), *BLK/EGR3* (E), *CD79A/EGR3* (H) and *PTPN6/EGR3* (I)  $\Delta C_T$  mean expression values.

implicated in therapy resistance [53, 54]. On the other hand, the undifferentiated phenotype of the BCR<sup>lo</sup> group could indicate a more aberrant oncogenic signaling program interfering with B-lineage gene expression networks. Nevertheless, the identification of four B-lineage genes whose expression reflects outcome enables early gene expression-based risk-stratification of patients.

That we identified both developmental proB stages at diagnosis and relapse with similar gene expression differences indicates preservation of the blast cell identity from diagnosis through the

minimal residual disease phase until relapse formation. Accordingly, it could well be that this cell identity is determined by the cell of origin, which is suggested to belong to the fetal liver-derived hematopoietic progenitor cell compartment [55–57]. However, further studies are needed to uncover mechanisms mediating the developmental arrest of blasts either in the pre-proB or proB stage.

In summary, analysis of the *EGR3* regulome of infant *KMT2A-r* iALL identified *EGR3* as a regulator of B-lineage commitment. Besides, our study presents four B-lineage genes with prognostic

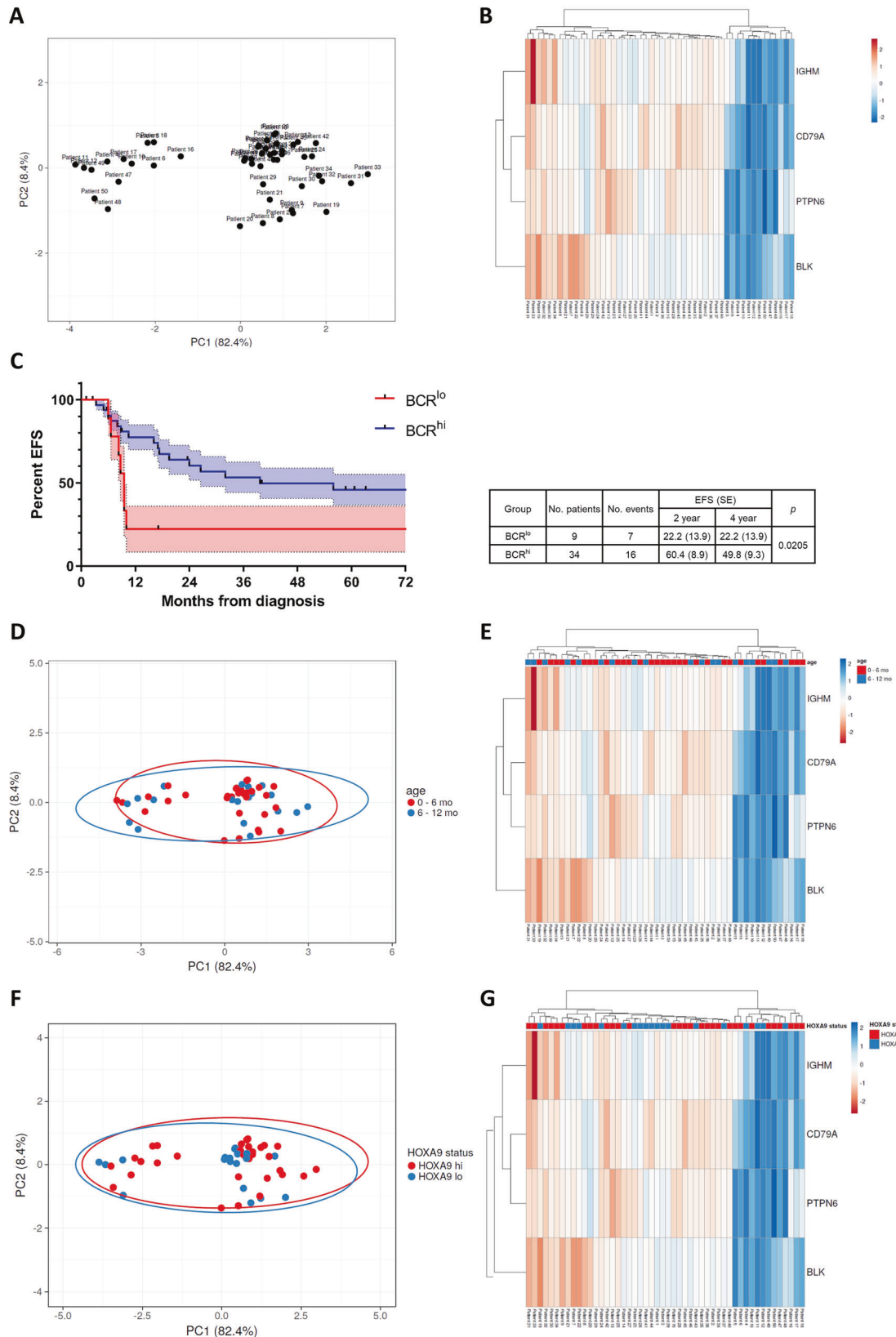


**Fig. 6 PCA and survival analysis of the diagnosis cohort.** **A** PCA of the diagnosis cohort among the *IGHM*, *CD79A*, *BLK*, and *PTPN6* expressions. PC1 represents 82.4% and PC2 8.4% of total variance, respectively. **B** Heatmap of the PCA visualizing bimodal clustering of patients. **C** Kaplan–Meier curves and log-rank test of the BCR<sup>lo</sup> (red) and BCR<sup>hi</sup> (blue) patients. S.E.M. of each curve is indicated in bright color. **D** PCA of the diagnosis cohort among the *IGHM*, *CD79A*, *BLK*, and *PTPN6* expressions with patients assigned to the age groups 0–6 months and 6–12 months. **E** Heatmap of the PCA visualizing bimodal clustering of patients is not affected by patient age at diagnosis. **F** PCA of the diagnosis cohort among the *IGHM*, *CD79A*, *BLK*, and *PTPN6* expressions with patients assigned to HOXA status groups *HOXA9* high (hi) and low (lo). **G** Heatmap of the PCA visualizing bimodal clustering of patients is not affected by HOXA status.

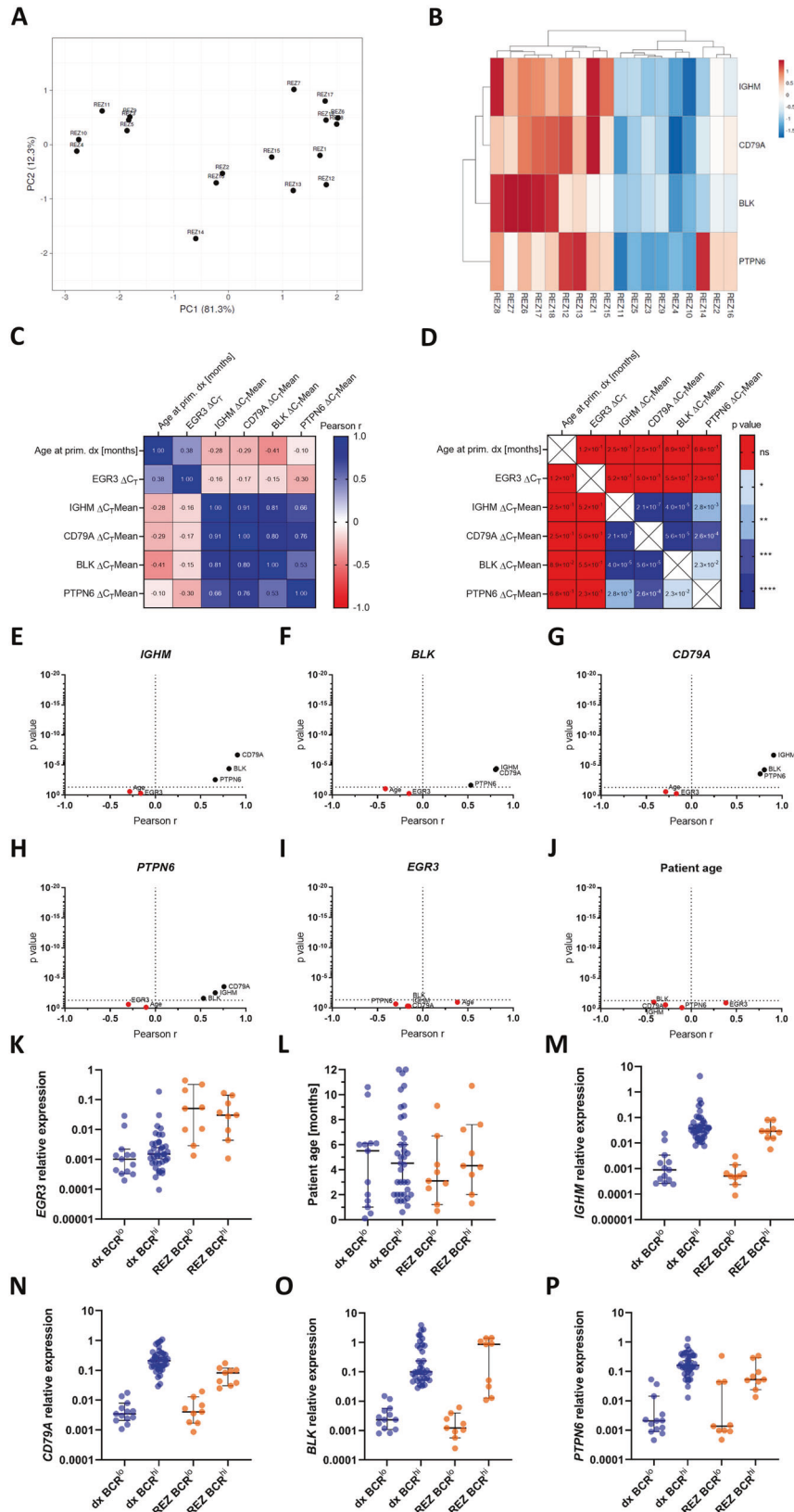


**Fig. 7 Patient clustering and Pearson correlation testing of the relapse cohort.** **A** PCA of the relapse cohort among the *IGHM*, *CD79A*, *BLK*, and *PTPN6* expressions. PC1 represents 81.3% and PC2 12.3% of total variance, respectively. **B** Heatmap of the PCA visualizing clustering of patients. Pearson correlation matrix indicating the Pearson *r* value (**C**) and *p* value (**D**) of all tested correlations. Volcano plots showing Pearson correlations of *IGHM* (**E**), *BLK* (**F**), *CD79A* (**G**), *PTPN6* (**H**), *EGR3* (**I**) and patient age (**J**). Correlations with  $p \geq 0.05$  were considered non-significant and marked in red. Comparison of the BCR<sup>lo</sup> and BCR<sup>hi</sup> groups of the diagnosis and relapse cohorts regarding *EGR3* relative expression (**K**), patient age (**L**), *IGHM* (**M**), *CD79A* (**N**), *BLK* (**O**) and *PTPN6* (**P**) relative expressions. Bars indicate the median and 95% confidence interval.

significance, suitable for gene expression-based risk stratification of *KMT2A-r* iALL patients.

## DATA AVAILABILITY

All generated datasets are available from the corresponding authors on reasonable request. MACE-Seq data are available at GEO with accession code GSE225710. ChIP-Seq data are available at GEO with accession code GSE205652.

## REFERENCES

- Pieters R, De Lorenzo P, Ancilffe P, Aversa LA, Brethon B, Biondi A, et al. Outcome of infants younger than 1 year with acute lymphoblastic leukemia treated with the interfant-06 protocol: results from an international phase III randomized study. *J Clin Oncol*. 2019;37:2246–56.
- Pieters R, Schrappe M, De Lorenzo P, Hann I, De Rossi G, Felice M, et al. A treatment protocol for infants younger than 1 year with acute lymphoblastic leukaemia (Interfant-99): an observational study and a multicentre randomised trial. *Lancet*. 2007;370:240–50.
- Meyer C, Burmeister T, Gröger D, Tsaar G, Fechina L, Renneville A, et al. The MLL recombinome of acute leukemias in 2017. *Leukemia*. 2018;32:273–84.
- Driessen EMC, de Lorenzo P, Campbell M, Felice M, Ferster A, Hann I, et al. Outcome of relapsed infant acute lymphoblastic leukemia treated on the interfant-99 protocol. *Leukemia*. 2016;30:1184–7.
- Kulp M, Siemund AL, Larghero P, Dietz A, Alten J, Cario G, et al. The immune checkpoint ICOSLG is a relapse-predicting biomarker and therapeutic target in infant t(4;11) acute lymphoblastic leukemia. *iScience*. 2022;25:104613.
- Beckmann AM, Wilce PA. Egr transcription factors in the nervous system. *Neurochem Int*. 1997;31:477–510.
- O'Donovan KJ, Levkovitz Y, Ahn D, Baraban JM. Functional comparison of Egr3 transcription factor isoforms: identification of an activation domain in the N-terminal segment absent from Egr3beta, a major isoform expressed in brain. *J Neurochem*. 2000;75:1352–7.
- Desmazières A, Decker L, Vallat JM, Charnay P, Gilardi-Hebenstreit P. Disruption of Krox20–Nab interaction in the mouse leads to peripheral neuropathy with biphasic evolution. *J Neurosci*. 2008;28:5891–900.
- Le N, Nagarajan R, Wang JYT, Svaren J, LaPash C, Araki T, et al. Nab proteins are essential for peripheral nervous system myelination. *Nat Neurosci*. 2005;8:932–40.
- Svaren J, Severson BR, Apel ED, Zimonjic DB, Popescu NC, Milbrandt J. NAB2, a corepressor of NGFI-A (Egr-1) and Krox20, is induced by proliferative and differentiative stimuli. *Mol Cell Biol*. 1996;16:3545–53.
- Swirloff AH, Apel ED, Svaren J, Severson BR, Zimonjic DB, Popescu NC, et al. Nab1, a corepressor of NGFI-A (Egr-1), contains an active transcriptional repression domain. *Mol Cell Biol*. 1998;18:512–24.
- Davis S, Bozon B, Laroche S. How necessary is the activation of the immediate early gene *zif268* in synaptic plasticity and learning? *Behav Brain Res*. 2003;142:17–30.
- Knapska E, Kaczmarek L. A gene for neuronal plasticity in the mammalian brain: *Zif268/Egr-1/NGFI-A/Krox-24/TIS8/ZENK*? *Prog Neurobiol*. 2004;74:183–211.
- Schneider-Maunoury S, Topilko P, Seitandou T, Levi G, Cohen-Tannoudji M, Pournin S, et al. Disruption of Krox-20 results in alteration of rhombomeres 3 and 5 in the developing hindbrain. *Cell*. 1993;75:1199–214.
- Williams J, Dragunow M, Lawlor P, Mason S, Abraham WC, Leah J, et al. Krox20 may play a key role in the stabilization of long-term potentiation. *Mol Brain Res*. 1995;28:87–93.
- Yamagata K, Kaufmann WE, Lanahan A, Papapavlou M, Barnes CA, Andreasson KI, et al. Egr3/Pilot, a zinc finger transcription factor, is rapidly regulated by activity in brain neurons and colocalizes with Egr1/zif268. *Learn Mem*. 1994;1:140–52.
- Cheng H, Hao S, Liu Y, Pang Y, Ma S, Dong F, et al. Leukemic marrow infiltration reveals a novel role for Egr3 as a potent inhibitor of normal hematopoietic stem cell proliferation. *Blood*. 2015;126:1302–13.
- Min IM, Pietramaggiore G, Kim FS, Passequé E, Stevenson KE, Wagers AJ. The transcription factor EGR1 controls both the proliferation and localization of hematopoietic stem cells. *Cell Stem Cell*. 2008;2:380–91.
- Carter JH, Lefebvre JM, Wiest DL, Tourtellotte WG. Redundant role for early growth response transcriptional regulators in thymocyte differentiation and survival. *J Immunol*. 2007;178:6796–805.
- Li S, Symonds ALJ, Zhu B, Liu M, Raymond MV, Miao T, et al. Early growth response Gene-2 (Egr-2) regulates the development of B and T cells. *PLoS One*. 2011;6:e18498.
- Ogbe A, Miao T, Symonds ALJ, Omodho B, Singh R, Bhullar P, et al. Early growth response Genes 2 and 3 regulate the expression of Bcl6 and differentiation of T follicular helper cells. *J Biol Chem*. 2015;290:20455–65.
- Metsalu T, Vilo J. ClustVis: a web tool for visualizing clustering of multivariate data using Principal Component Analysis and heatmap. *Nucleic Acids Res*. 2015;43:W566–570.
- Subramanian A, Tamayo P, Mootha VK, Mukherjee S, Ebert BL, Gillette MA, et al. Gene set enrichment analysis: a knowledge-based approach for interpreting genome-wide expression profiles. *Proc Natl Acad Sci USA*. 2005;102:15545–50.
- Wang S, Sun H, Ma J, Zang C, Wang C, Wang J, et al. Target analysis by integration of transcriptome and ChIP-seq data with BETA. *Nat Protoc*. 2013;8:2502–15.
- Mi H, Muruganujan A, Huang X, Ebert D, Mills C, Guo X, et al. Protocol Update for large-scale genome and gene function analysis with the PANTHER classification system (v.14.0). *Nat Protoc*. 2019;14:703–21.
- Bagger FO, Kinalis S, Rapin N. BloodSpot: a database of healthy and malignant haematopoiesis updated with purified and single cell mRNA sequencing profiles. *Nucleic Acids Res*. 2019;47:D881–5.
- Kohlmann A, Kipps TJ, Rassenti LZ, Downing JR, Shurtleff SA, Mills KI, et al. An international standardization programme towards the application of gene expression profiling in routine leukaemia diagnostics: the Microarray Innovations in LLeukemia study prephase. *Br J Haematol*. 2008;142:802–7.
- Novershtern N, Subramanian A, Lawton LN, Mak RH, Haining WN, McConkey ME, et al. Densely interconnected transcriptional circuits control cell states in human hematopoiesis. *Cell*. 2011;144:296–309.
- Gillespie M, Jassal B, Stephan R, Milacic M, Rothfels K, Senff-Ribeiro A, et al. The reactome pathway knowledgebase 2022. *Nucleic Acids Res*. 2022;50:D687–92.
- Martens M, Ammar A, Riutta A, Waagmeester A, Slenker DN, Hanspers K, et al. WikiPathways: connecting communities. *Nucleic Acids Res*. 2021;49:D613–21.
- Schaefer CF, Anthony K, Krupa S, Buchoff J, Day M, Hannay T, et al. PID: the pathway interaction database. *Nucleic Acids Res*. 2009;37:D674–9.
- Höllbacher B, Balázs K, Heinig M, Uhlenhaut NH. Seq-ing answers: current data integration approaches to uncover mechanisms of transcriptional regulation. *Comput Struct Biotechnol J*. 2020;18:1330–41.
- Bullerwell CE, Robichaud PP, Deprez PML, Joy AP, Wajnberg G, D'Souza D, et al. EBF1 drives hallmark B cell gene expression by enabling the interaction of PAX5 with the MLL H3K4 methyltransferase complex. *Sci Rep*. 2021;11:1537.
- Calderón L, Schindler K, Malin SG, Schebesta A, Sun Q, Schwickert T, et al. Pax5 regulates B cell immunity by promoting PI3K signaling via PTEN down-regulation. *Sci Immunol*. 2021;6:eabg5003.
- Cobaleda C, Schebesta A, Delogu A, Busslinger M. Pax5: the guardian of B cell identity and function. *Nat Immunol*. 2007;8:463–70.
- Li S, Miao T, Sebastian M, Bhullar P, Ghaffari E, Liu M, et al. The transcription factors Egr2 and Egr3 are essential for the control of inflammation and antigen-induced proliferation of B and T cells. *Immunity*. 2012;37:685–96.
- Fuxa M, Busslinger M. Reporter gene insertions reveal a strictly B lymphoid-specific expression pattern of Pax5 in support of its B cell identity function. *J Immunol*. 2007;178:3031–7.
- Horcher M, Souabni A, Busslinger M. Pax5/BSAP maintains the identity of B cells in late B lymphopoiesis. *Immunity*. 2001;14:779–90.
- Nutt SL, Heavey B, Rolink AG, Busslinger M. Commitment to the B-lymphoid lineage depends on the transcription factor Pax5. *Nature*. 1999;401:556–62.
- Revilla-I-Domingo R, Bilic I, Vilagos B, Tagoh H, Ebert A, Tamir IM, et al. The B-cell identity factor Pax5 regulates distinct transcriptional programmes in early and late B lymphopoiesis. *EMBO J*. 2012;31:3130–46.
- McManus S, Ebert A, Salvaggio G, Medvedovic J, Sun Q, Tamir I, et al. The transcription factor Pax5 regulates its target genes by recruiting chromatin-modifying proteins in committed B cells. *EMBO J*. 2011;30:2388–404.
- Jackson TR, Ling RE, Roy A. The origin of B-cells: human fetal B cell development and implications for the pathogenesis of childhood acute lymphoblastic leukemia. *Front Immunol*. 2021 [cited 2022 Dec 5];12. Available from: <https://www.frontiersin.org/articles/10.3389/fimmu.2021.637975>.
- LeBien TW. Fates of human B-cell precursors. *Blood*. 2000;96:9–23.
- Gardner R, Wu D, Cherian S, Fang M, Hanafi LA, Finney O, et al. Acquisition of a CD19-negative myeloid phenotype allows immune escape of MLL-rearranged B-ALL from CD19 CAR-T-cell therapy. *Blood*. 2016;127:2406–10.
- Mejstříková E, Hrusak O, Borowitz MJ, Whitlock JA, Brethon B, Trippett TM, et al. CD19-negative relapse of pediatric B-cell precursor acute lymphoblastic leukemia following blinatumomab treatment. *Blood Cancer J*. 2017;7:1–5.
- Rayes A, McMasters RL, O'Brien MM. Lineage switch in MLL-rearranged infant leukemia following CD19-directed therapy. *Pediatr Blood Cancer*. 2016;63:1113–5.
- Tirtakusuma R, Szolysek K, Milne P, Grinev VV, Ptasinska A, Chin PS, et al. Epigenetic regulator genes direct lineage switching in MLL/AF4 leukemia. *Blood*. 2022;140:1875–90.
- Baron VT, Pio R, Jia Z, Mercola D. Early Growth Response 3 regulates genes of inflammation and directly activates IL6 and IL8 expression in prostate cancer. *Br J Cancer*. 2015;112:755–64.

49. Healy S, Khan P, Davie JR. Immediate early response genes and cell transformation. *Pharmacol Ther.* 2013;137:64–77.
50. O'Byrne S, Elliott N, Rice S, Buck G, Fordham N, Garnett C, et al. Discovery of a CD10-negative B-progenitor in human fetal life identifies unique ontogeny-related developmental programs. *Blood.* 2019;134:1059–71.
51. Boller S, Grosschedl R. The regulatory network of B-cell differentiation: a focused view of early B-cell factor 1 function. *Immunol Rev.* 2014;261:102–15.
52. Sanz E, Muñoz-A N, Monserrat J, Van-Den-Rym A, Escoll P, Ranz I, et al. Ordering human CD34+CD10-CD19+ pre/pro-B-cell and CD19- common lymphoid progenitor stages in two pro-B-cell development pathways. *Proc Natl Acad Sci USA.* 2010;107:5925–30.
53. Chen C, Yu W, Alikarami F, Qiu Q, Chen CH, Flournoy J, et al. Single-cell multiomics reveals increased plasticity, resistant populations, and stem-cell-like blasts in KMT2A-rearranged leukemia. *Blood.* 2022;139:2198–211.
54. Liao W, Kohler ME, Fry T, Ernst P. Does lineage plasticity enable escape from CAR-T cell therapy? Lessons from MLL-r leukemia. *Exp Hematol.* 2021;50301-472X:00248–4.
55. Agraz-Doblas A, Bueno C, Bashford-Rogers R, Roy A, Schneider P, Bardini M, et al. Unraveling the cellular origin and clinical prognostic markers of infant B-cell acute lymphoblastic leukemia using genome-wide analysis. *Haematologica.* 2019;104:1176–88.
56. Khabirova E, Jardine L, Coorens THH, Webb S, Treger TD, Engelbert J, et al. Single-cell transcriptomics reveals a distinct developmental state of KMT2A-rearranged infant B-cell acute lymphoblastic leukemia. *Nat Med.* 2022;28:743–751.
57. Rice S, Jackson T, Crump NT, Fordham N, Elliott N, O'Byrne S, et al. A human fetal liver-derived infant MLL-AF4 acute lymphoblastic leukemia model reveals a distinct fetal gene expression program. *Nat Commun.* 2021;12:6905.

## ACKNOWLEDGEMENTS

We thank Birthe Fedders for sample composition and sending, the Center for Biological Resources (CRB-cancer; BB-0033-00076), Robert Debré Hospital, France, and our lab colleagues for impactful discussions.

## AUTHOR CONTRIBUTIONS

MK wrote the manuscript; MK, PL, HB, CM, MAR, and RM planned and interpreted experiments; MK performed GSEA and qRT-PCR; MK, TS, and MAR performed flow cytometry; PL conducted binding and expression target analysis; HB, CM, and PL helped to write the manuscript; JA, GC, CE, ACE, HC, MB, GiC, PDL, and MGv provided patient samples and outcome data, and helped to analyze clinical data; RM provided funding; all authors reviewed and approved the manuscript.

## FUNDING

This work has been funded in part by DFG grant MA 1876/12-1 and Wilhelm Sander foundation grant 2020.070 to RM, and in part by ERA-NET TRANSCAN EJC, Foundation ARC, France to HC. Open Access funding enabled and organized by Projekt DEAL.

## COMPETING INTERESTS

The authors declare no competing interests.

## ADDITIONAL INFORMATION

**Supplementary information** The online version contains supplementary material available at <https://doi.org/10.1038/s41375-023-01895-z>.

**Correspondence** and requests for materials should be addressed to Marius Külp or Rolf Marschalek.

**Reprints and permission information** is available at <http://www.nature.com/reprints>

**Publisher's note** Springer Nature remains neutral with regard to jurisdictional claims in published maps and institutional affiliations.



**Open Access** This article is licensed under a Creative Commons Attribution 4.0 International License, which permits use, sharing, adaptation, distribution and reproduction in any medium or format, as long as you give appropriate credit to the original author(s) and the source, provide a link to the Creative Commons license, and indicate if changes were made. The images or other third party material in this article are included in the article's Creative Commons license, unless indicated otherwise in a credit line to the material. If material is not included in the article's Creative Commons license and your intended use is not permitted by statutory regulation or exceeds the permitted use, you will need to obtain permission directly from the copyright holder. To view a copy of this license, visit <http://creativecommons.org/licenses/by/4.0/>.

© The Author(s) 2023